

# A photometric study of the Open Cluster II: Stellar population and dynamical evolution in NGC 559

Y. C. Joshi<sup>1\*</sup>, L. A. Balona<sup>2</sup>, S. Joshi<sup>1</sup>, B. Kumar<sup>1</sup>,

<sup>1</sup>*Aryabhata Research Institute of Observational Sciences (ARIES), Manora peak, Nainital, India*

<sup>2</sup>*South African Astronomical Observatory, PO Box 9, Observatory 7935, Cape Town, South Africa*

Accepted 07 October 2013 Received 22 July 2013

## ABSTRACT

We present *UBVRI* photometry of stars in the field of the intermediate-age open cluster NGC 559. By determining the stellar membership probabilities derived through a photometric and kinematic study of the cluster, we identify the 22 most probable cluster members. These are used to obtain robust cluster parameters. The mean proper motion of the cluster is  $\mu_x = -3.29 \pm 0.35$ ,  $\mu_y = -1.24 \pm 0.28$  mas yr<sup>-1</sup>. The radial distribution of the stellar surface density gives a cluster radius of  $4'.5 \pm 0'.2$  ( $3.2 \pm 0.2$  pc). By fitting solar metallicity stellar isochrones to the colour-colour and colour-magnitude diagrams, we find a uniform cluster reddening of  $E(B - V) = 0.82 \pm 0.02$ . The cluster has an age of  $224 \pm 25$  Myr and is at a distance of  $2.43 \pm 0.23$  kpc. From the optical and near-infrared two-colour diagrams, we obtain colour excesses in the direction of the cluster  $E(V - K) = 2.14 \pm 0.02$ ,  $E(J - K) = 0.37 \pm 0.01$ , and  $E(B - V) = 0.76 \pm 0.04$ . A total-to-selective extinction of  $R_V = 3.5 \pm 0.1$  is found in the direction of the cluster which is marginally higher than the normal value. We derive the luminosity function and the mass function for the cluster main sequence. The mass function slope is found to be  $-2.12 \pm 0.31$ . We find evidence of mass segregation in this dynamically relaxed cluster.

**Key words:** open cluster:individual:NGC 559–stars: formation – stars: luminosity function, mass function–techniques:photometric

## 1 INTRODUCTION

Systematic photometric studies of Galactic open star clusters (OCs) offer unique opportunities to understand large-scale star formation processes in the Galaxy and in Galactic clusters (Lada 2003). The precise knowledge of cluster parameters such as age, distance, reddening and chemical composition as well as knowledge of the stellar population distribution and the cluster mass function at the time of star formation play a key role in understanding the star formation history. The importance of photometric studies of OCs lies in the colour-colour and colour-magnitude diagrams derived through multi-band photometric observations. Since most of the OCs are embedded in the Galactic disk and are likely to be affected by field star contamination, it is essential to discriminate between members and non-members of the clusters. The amount of field star contamination depends on the location of the cluster. It is necessary to perform a detailed membership analysis of the stars found within the

observed field for a robust investigation of cluster properties (Carraro et al. 2008, Yadav et al. 2008). For most of the OCs, kinematical data is unavailable. However, recent all-sky proper motion catalogues (e.g., Roeser et al. 2010, Zacharias et al. 2013), provide clues to determine cluster membership. Together with a photometric study of the cluster, it becomes possible to draw some conclusions regarding the dynamical evolution of the cluster.

At ARIES, Nainital, we have been carrying out a long-term observational program to search and characterize the variable stars in Galactic open star clusters using various 1- to 2-m class telescopes in India. The advantage of having such observations is that they can also be used to study the physical properties of the clusters and their stellar and dynamical evolution. In Joshi et al. (2012), we performed a photometric study of the intermediate age open cluster, NGC 6866, which also included a search for variable stars in the cluster. The results presented here for NGC 559 are a continuation of our efforts to understand star formation in some unstudied or poorly studied young- and intermediate-age open clusters.

\* E-mail: yogesh@aries.res.in

NGC 559 (RA = 01:29:35, DEC = +63:18:14;  $l = 127^\circ.2, b = +0^\circ.75$ ) is a moderately populated and heavily reddened intermediate-age open cluster, classified as type I2*m* by Trumpler (1930) and II2*m* by Ruprecht (1966). It is located in the direction of the second Galactic Quadrant in the vicinity of the Perseus and Local arms (Russeil et al. 2007). Photoelectric photometry of the cluster was obtained by Lindoff (1969) and Jennens & Helfer (1975), while Grubbisich (1975) provided photographic photometry of cluster stars. A subsequent investigation using CCD photometry was carried out by Ann & Lee (2002, hereafter AL02) and Maciejewski & Niedzieski (2007, hereafter MN07). However, a complete UBVR study is still lacking. Moreover, there has not been any systematic attempt to identify cluster members in the field of this cluster.

The main focus of the present study is to accurately determine the fundamental parameters of NGC 559 by identifying cluster members using photometric and kinematic criteria. The outline of the paper is as follows. A photometric study of the cluster is presented in §2. The cluster properties are discussed in §3 and fundamental parameters are derived in §4. The dynamical study of the cluster is presented in §5. Finally, we discuss the results in §6.

## 2 PHOTOMETRIC STUDY OF THE CLUSTER

### 2.1 Observations and Calibration

Johnson-Cousins *UBVRI* photometry of stars in the field of NGC 559 was obtained on 2010, November 30 using the 1-m Sampurnanand telescope at Nainital, India. The telescope is equipped with a  $2k \times 2k$  CCD camera which covers a  $\sim 13' \times 13'$  field of view. We acquired two frames each in *U*, *B*, *V*, *R* and *I* filters with exposure times of 300, 300, 200, 100, and 60-sec in respective passbands, respectively, at a typical airmass of about 1.3. On the same night we also observed two Landolt's standard fields: SA95 and PG0231+051 (Landolt 1992) at different airmasses. The usual image processing procedures were performed which included bias subtraction, flat fielding, and cosmic ray removal. We used the IRAF<sup>1</sup> software package for this purpose.

Photometry of the frames was performed using the DAOPHOT II profile fitting software (Stetson 1987). Details of the photometric calibration obtained on this night are given in Joshi et al. (2012). Transformation coefficients for the standard stars were determined as follows.

$$\begin{aligned} u &= U + 8.16 \pm 0.01 - (0.05 \pm 0.01)(U - B) + (0.55 \pm 0.02)X \\ b &= B + 5.81 \pm 0.02 - (0.01 \pm 0.02)(B - V) + (0.29 \pm 0.03)X \\ v &= V + 5.43 \pm 0.01 - (0.08 \pm 0.01)(B - V) + (0.15 \pm 0.01)X \\ r &= R + 5.23 \pm 0.01 - (0.09 \pm 0.02)(V - R) + (0.09 \pm 0.02)X \\ i &= I + 5.63 \pm 0.02 + (0.01 \pm 0.01)(R - I) + (0.07 \pm 0.02)X \end{aligned}$$

where  $u, b, v, r$  and  $i$  are the aperture instrumental magnitudes and  $U, B, V, R$  and  $I$  are the standard magni-

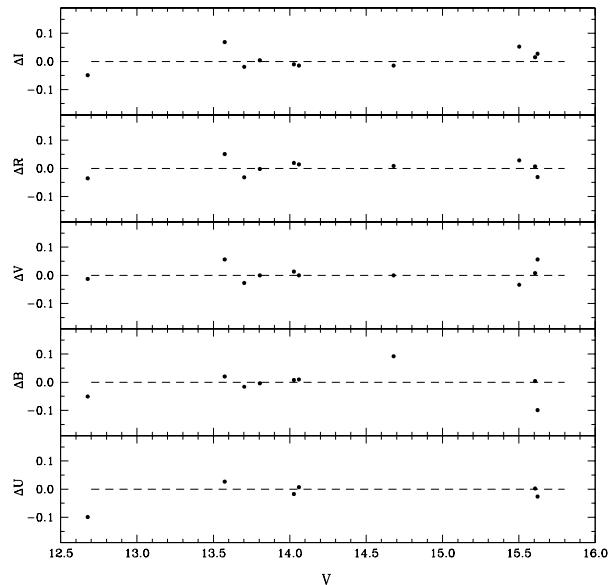


**Figure 1.** For the standard stars in the Landolt field, plots show residuals of the differential magnitudes (standard - calibrated) in the *U*, *B*, *V*, *R*, and *I* bands as a function of *V* magnitude. The dashed line drawn in each panel represents a zero difference.

**Table 1.** Average internal photometric errors per magnitude bin as a function of brightness.

mag	$\sigma_U$	$\sigma_B$	$\sigma_V$	$\sigma_R$	$\sigma_I$
10–11	-	-	0.02	0.02	0.01
11–12	0.01	0.01	0.01	0.01	0.01
12–13	0.02	0.01	0.01	0.01	0.01
13–14	0.01	0.00	0.01	0.01	0.01
14–15	0.01	0.01	0.01	0.01	0.01
15–16	0.01	0.01	0.01	0.01	0.02
16–17	0.02	0.01	0.01	0.01	0.02
17–18	0.04	0.01	0.02	0.02	0.04
18–19	0.08	0.02	0.03	0.03	0.07
19–20	0.20	0.04	0.06	0.06	0.20
20–21	-	0.07	0.11	0.13	-
21–22	-	0.21	0.26	-	-

tudes and  $X$  is the airmass. The difference between the calibrated magnitudes derived from the above transformation equations and the Landolt (1992) magnitudes are plotted in Fig. 1. The standard deviations of these measurements are estimated to be 0.04, 0.05, 0.03, 0.03, and 0.03 mag for the *U*, *B*, *V*, *R* and *I* filters, respectively. The above transformation coefficients were used to convert instrumental magnitudes to the standard system. The average internal photometric error per magnitude bin in all the five filters on the night of standardization are listed in Table 1. This shows that photometric errors become large ( $> 0.1$  mag) for stars fainter than  $V \approx 20$  mag. To standardize the data on remaining nights, differential photometry was performed using a linear fit between the standard and instrumental magnitudes on each night, assuming that most of the stars are non-variable.

<sup>1</sup> Image Reduction and Analysis Facility (IRAF) is distributed by the National Optical Astronomy Observatories, which are operated by the Association of Universities for Research in Astronomy, Inc., under cooperative agreement with the National Science Foundation.

**Table 2.** Completeness Factor of the photometric data in  $U$ ,  $B$ ,  $V$ ,  $R$  and  $I$  bands in cluster and field regions.

mag range	$U$		$B$		$V$		$R$		$I$	
	cluster	field	cluster	field	cluster	field	cluster	field	cluster	field
10–11	-	-	-	-	-	-	1.00	1.00	0.83	0.83
11–12	1.00	1.00	1.00	1.00	0.94	1.00	1.00	1.00	1.00	1.00
12–13	1.00	0.96	1.00	1.00	1.00	1.00	1.00	0.95	0.97	1.00
13–14	1.00	1.00	1.00	1.00	1.00	0.96	1.00	1.00	0.95	1.00
14–15	0.95	1.00	1.00	0.96	1.00	1.00	0.90	1.00	1.00	0.97
15–16	0.97	1.00	1.00	1.00	0.97	1.00	0.97	0.96	0.97	0.97
16–17	0.97	0.97	0.97	1.00	0.93	1.00	0.97	0.97	0.89	0.92
17–18	1.00	0.97	0.93	1.00	1.00	0.97	0.90	0.97	0.89	0.88
18–19	0.65	0.70	1.00	0.94	0.93	0.97	0.82	0.83	0.46	0.51
19–20	0.19	0.20	0.90	0.94	0.86	0.91	0.72	0.73	-	-
20–21	-	-	0.45	0.52	0.48	0.52	0.09	0.16	-	-

## 2.2 Completeness of the data

It is necessary to determine the completeness of the data as it is not always possible to detect every star in the CCD frame, particularly the faintest stars. The completeness factor (CF) is required in order to derive the luminosity function and the mass function of the cluster as well as to estimate the stellar density distribution. The `ADDSTAR` routine in `DAOPHOT` was used to determine CF. This involves adding randomly selected artificial stars with different, but known, magnitudes and positions to the original frames. We added about 10–15% of the actually detected stars, so that the crowding characteristics of the original image is almost unchanged. We added simulated stars to all bands in such a way that they have similar geometric locations. We varied the brightness of the artificial star depending on its location relative to the Main-Sequence (MS) in the  $V$  band. We constructed five frames for each passband and re-processed them with the same procedure as used in the original frames. The average ratio of number of stars recovered to the number of simulated stars in the different magnitude bins gives the CF as a function of magnitude. The CF in all five passbands for both cluster and field regions is given in Table 2. From the table, one can see that the completeness decreases towards the fainter stars because of the increased crowding caused by the large number of low-mass stars.

## 2.3 Astrometry

In order to transform CCD pixel coordinates to celestial coordinates, we used the on-line digitized ESO catalogue included in the `skycat` software as an absolute astrometric reference frame. A linear astrometric solution was derived for the  $V$  filter reference frame by matching positions of 63 well isolated, bright stars in the USNOA2.0 catalogue. The `ccmap` and `cctran` routines in `IRAF` were used to find a transformation equation which gives the celestial coordinates  $(\alpha, \delta)$  as a function of the pixel coordinates,  $(X, Y)$ . The resulting celestial coordinates have standard deviations of 0.1 arcsec in both right ascension and declination.

A finding chart for stars in NGC 559 is shown in Fig. 2. We do not see any significant concentration of stars at the center which suggests that cluster is loosely bound.

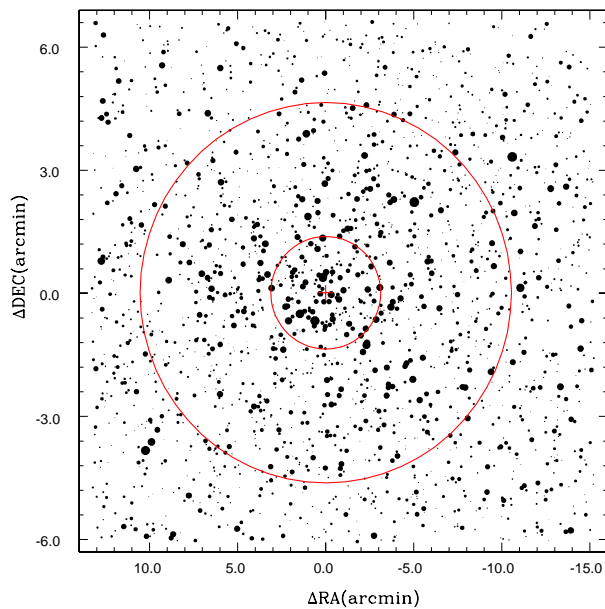


**Figure 2.** Finding chart of stars in the field of NGC 559. North is upwards and East is on the left. The sizes of the filled circles are proportional to the brightness of the stars in the  $V$  band. The faintest are  $V = 21$ . The inner and outer rings indicate core and cluster radii with origin,  $(0, 0)$ , at the cluster center.

## 2.4 Comparison with previous photometry

Photoelectric and photographic observations of NGC 559 have been carried out by Lindoff (1969) and Grubbisich (1975) respectively. Photographic magnitudes contain relatively large errors, while photoelectric magnitudes are mostly confined to stars brighter than  $V \sim 15$ , hence we did not compare them with our photometry in the present study. CCD photometry in the  $UBVRI$  bands is discussed in AL02, but these data have not been published. Recently, MN07 performed a wide field CCD survey of a few clusters using a 90/180 cm Schmidt-Cassegrain telescope equipped with a SBIG camera. This survey also includes NGC 559, for which  $BV$  data are presented, but only for stars brighter than about 18 mag.

We found 1112 stars in the MN07 catalogue which are included in our study. However, there are only 687 stars in

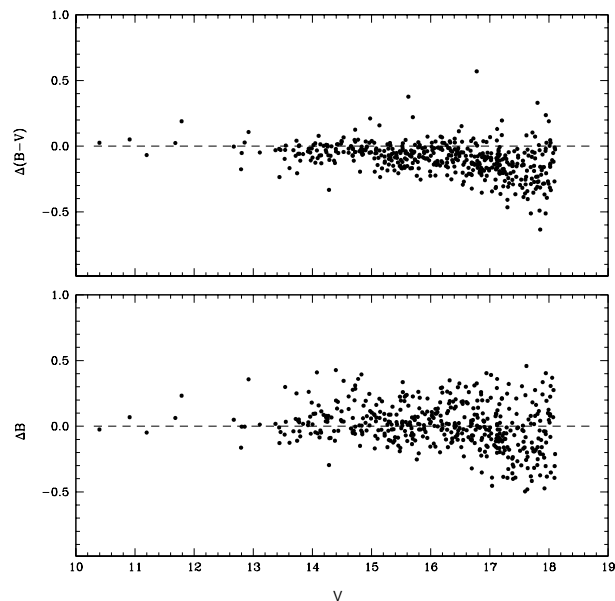


**Figure 3.** Differences,  $\Delta$  between measurements presented in MN07 and in the present study for  $B$  magnitude and  $(B - V)$  colour. Zero difference is indicated by the dashed line.

**Table 3.** Differences in  $B$  and  $(B - V)$  between MN07 and present study. The standard deviation in the difference for each magnitude bin is also given in the bracket.

V mag range	$\Delta B$	$\Delta(B-V)$
10–11	0.02 (0.05)	0.04 (0.01)
11–12	0.08 (0.12)	0.05 (0.11)
12–13	0.05 (0.17)	-0.02 (0.09)
13–14	0.03 (0.11)	-0.06 (0.06)
14–15	0.07 (0.14)	-0.03 (0.07)
15–16	0.02 (0.12)	-0.07 (0.09)
16–17	0.03 (0.15)	-0.09 (0.11)
17–18	-0.08 (0.20)	-0.17 (0.15)
18–19	-0.09 (0.24)	-0.21 (0.20)

common for which both  $B$  and  $V$  magnitudes are available. We have cross-identified stars in the two catalogues on the assumption that stars are correctly matched if the difference in position is less than  $1''$ . On this basis, we found 505 stars in common which have similar  $B$  and  $V$  magnitudes within 0.5 mag. A comparison of  $B$  magnitudes and  $(B - V)$  colours between the two catalogues is shown in Fig. 3. The mean difference and standard deviation in each magnitude bin is given in Table 3. This shows that our  $B$  measurements are in fair agreement with those given in the MN07 catalogue. However, there is a systematic difference in  $(B - V)$  colours between the two catalogues.

### 2.5 A complete *UBVRIJHK*-proper motion catalog

We have compiled a photometric catalogue of 2393 stars in the field of NGC 559. The catalogue contains 515, 1288, 2177, 2352 and 2221 stars measured in the *UBVRI* bands respectively. Near-infrared magnitudes for point sources

around NGC 559 have also been obtained from the Two Micron All-sky survey (2MASS; Skrutskie et al. 2006). The 2MASS provides photometry in the  $J$  ( $1.25 \mu\text{m}$ ),  $H$  ( $1.65 \mu\text{m}$ ) and  $K_s$  ( $2.17 \mu\text{m}$ ) bands up to a limiting magnitude of 15.8, 15.1, and 14.3 respectively. We found  $JHK_s$  magnitudes for 917 stars in the field of NGC 559, of which 906 stars are identified in our catalogue within  $1''$  of their positions. The  $K_s$  magnitudes were converted into  $K$  magnitudes using equations given in the Carpenter et al. (2001). The proper motions have been taken from Roeser et al. (2010) which gives a catalogue for about 900 million stars derived from the USNOB1.0 and 2MASS all sky catalogues.

The *UBVRIJHK* magnitudes and proper motions, wherever measured, are presented in Table 4, sorted in increasing order of  $V$ . In the catalogue, column 1 contains a running number, columns 2 and 3 give right ascension and declination for J(2000), columns 4 to 11 provide photometric magnitudes and corresponding errors in the *UBVRIJHK* passbands. The proper motion along the RA and DEC directions and their respective errors are given in the columns 12 and 13. Only a short extract of Table 4 is shown; the complete catalogue is available at the WEBDA open cluster data base website<sup>2</sup> or can be obtained directly from the authors.

## 3 STRUCTURAL PROPERTIES OF THE CLUSTER

### 3.1 Spatial Structure: Radial density profile

The spatial structure and precise center of the star cluster is difficult to determine due to the irregular shape of the cluster and the non-uniform distribution of stars at different brightness levels. We define the cluster centre as the region where maximum stellar density is attained. To determine this value, we consider all stars with  $V < 19$  for which the completeness level is in excess of 90%. We found that the stellar density peaks at the pixel coordinate (510, 535), corresponding to a cluster centre at  $(\alpha, \delta) = (01:29:32.33, +63:18:14.5)$ . An error of up to  $10''$  is expected in locating the cluster center.

To draw the radial density profile (RDP), we determined the stellar density in concentric rings,  $0'.5$  wide, centered on the cluster center. The errorbars were derived assuming Poisson statistics. We fitted a King (1966) stellar density as modified by Kaluzny & Udalski (1992):

$$\rho(r) = \rho_f + \frac{\rho_0}{1 + (\frac{r}{r_c})^2}$$

Here  $\rho_f$  is the field density and  $r_c$  is the core radius of cluster where the stellar density,  $\rho(r)$ , becomes half of its central value,  $\rho_0$ . The stellar density distribution in the  $V$  band is shown in Fig. 4. A  $\chi^2$  best fit to the radial density profile is shown in the figure along with the field star density. The cluster boundary is considered to be the point in the radial direction when  $\rho(r)$  falls below the field star density by  $3\sigma$ . The value of the core radius was found to be  $1'.3 \pm 0'.3$  and the cluster radius was estimated to be  $4'.5 \pm 0'.2$ . Our radius estimate is the same as that determined by AL02.

<sup>2</sup> <http://obswww.unige.ch/webda/>

1	01:29:12.19	+63:20:28.1	10.952±0.002	10.838±0.004	10.397±0.032	10.188±0.011	9.838±0.004	9.595±0.021	9.446±0.026	9.418±0.022	-11.5±1.9	3.4±1.9
2	01:28:49.96	+63:21:34.2	11.295±0.011	11.016±0.009	10.459±0.027	-	9.729±0.026	9.378±0.023	9.181±0.028	9.117±0.020	9.9±1.9	4.6±1.9
3	01:29:34.77	+63:17:34.3	11.448±0.011	11.484±0.004	10.908±0.012	10.552±0.014	10.233±0.006	9.856±0.021	9.576±0.024	9.550±0.024	10.5±1.9	3.0±1.9
4	01:30:13.25	+63:14:24.7	14.340±0.012	12.819±0.004	11.196±0.014	10.257±0.020	9.369±0.019	8.139±0.017	7.358±0.039	7.210±0.005	7.8±2.7	-7.8±2.7
5	01:29:38.19	+63:17:44.6	12.814±0.010	12.539±0.002	11.680±0.008	11.198±0.009	10.774±0.006	-	-	-	27.5±2.7	-1.3±2.7
6	01:29:32.98	+63:18:37.5	12.195±0.019	12.377±0.022	11.787±0.008	11.431±0.009	11.029±0.012	-	-	-	-12.3±4.5	-4.0±4.6
7	01:28:48.12	+63:18:22.6	12.165±0.021	-	11.928±0.006	-	11.146±0.020	-	-	-	-4.9±3.1	-6.7±3.1
8	01:29:23.07	+63:16:58.7	17.131±0.027	14.780±0.006	12.382±0.007	10.207±0.017	-	5.797±0.015	4.707±0.015	4.264±0.013	-4.6±14.1	-76.0±14.1
9	01:30:11.87	+63:14:37.2	13.552±0.012	13.424±0.007	12.670±0.009	12.214±0.011	11.759±0.021	-	-	-	20.9±4.9	-4.3±5.1
10	01:29:36.72	+63:22:08.0	17.523±0.038	14.927±0.011	12.792±0.009	11.457±0.020	10.065±0.005	8.460±0.021	7.518±0.037	7.215±0.027	0.8±5.0	-1.3±5.0
11	01:30:23.27	+63:19:02.0	16.061±0.012	14.477±0.010	12.804±0.011	11.796±0.009	10.777±0.016	9.496±0.019	8.771±0.028	8.575±0.020	10.8±19.6	-65.4±19.6
12	01:29:36.36	+63:20:06.9	13.941±0.005	13.571±0.003	12.853±0.008	12.445±0.011	11.951±0.007	11.369±0.017	11.136±0.024	11.057±0.022	-1.3±2.7	8.0±2.7
13	01:29:17.49	+63:17:54.5	-	14.537±0.016	12.920±0.010	11.964±0.009	10.977±0.007	9.702±0.021	9.002±0.026	8.792±0.022	15.4±25.7	-51.8±25.7
14	01:29:40.77	+63:17:34.6	16.577±0.015	14.922±0.004	13.109±0.009	12.031±0.010	10.935±0.007	9.561±0.019	8.730±0.026	8.510±0.022	-8.6±14.1	-23.7±14.1
15	01:29:12.54	+63:16:08.6	15.026±0.013	14.467±0.004	13.375±0.006	12.720±0.010	11.951±0.007	11.063±0.019	10.663±0.026	10.519±0.024	-5.5±4.0	-0.6±4.0
16	01:29:20.05	+63:18:23.1	14.511±0.013	14.150±0.008	13.431±0.011	12.999±0.011	12.471±0.014	11.807±0.021	11.628±0.028	11.492±0.026	-12.0±4.0	-1.5±4.0
17	01:28:39.03	+63:15:58.0	15.158±0.010	14.455±0.011	13.437±0.014	12.862±0.016	12.198±0.014	-	-	-	34.0±4.0	0.8±4.0
18	01:29:31.07	+63:18:12.5	16.387±0.016	15.061±0.004	13.442±0.009	12.491±0.011	11.514±0.007	10.282±0.019	9.583±0.024	9.400±0.022	-10.8±6.4	-2.2±6.4
19	01:29:32.99	+63:19:35.4	14.719±0.008	14.293±0.004	13.460±0.008	12.960±0.010	12.394±0.010	11.707±0.019	11.456±0.024	11.353±0.024	-2.2±4.0	-5.1±4.0
20	01:29:46.02	+63:19:27.0	17.038±0.026	15.350±0.005	13.529±0.007	12.427±0.007	11.306±0.009	9.877±0.019	9.076±0.024	8.861±0.022	-2.3±5.0	0.0±5.0
2392	01:29:14.55	+63:20:49.8	-	-	-	19.632±0.101	18.148±0.064	-	-	-	-	-
2393	01:29:11.31	+63:18:23.3	-	-	-	19.324±0.073	18.267±0.048	-	-	-	-	-

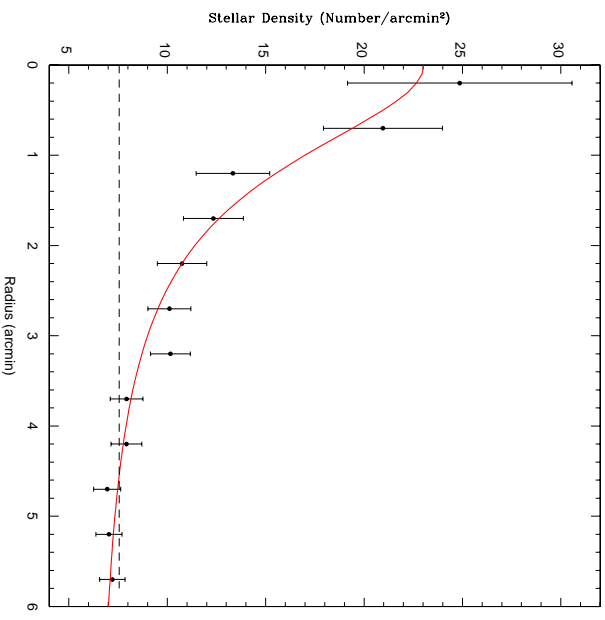


**Figure 4.** The stellar density distribution in NGC 559 for stars brighter than 19 mag. The solid line represents the King profile while the horizontal dashed line indicates the field density.

The inner and outer rings in Fig. 2 represent the core and cluster regions, respectively.

We noticed that the core radii derived from bright stars is smaller than those which include stars up to  $V=20$ . This suggests that: i) the core and cluster radii derived using the RDP are only approximate or, ii) that there is mass segregation due to the dynamical evolution of the cluster. In the latter case, it would seem that bright massive stars move towards the cluster centre, while faint low-mass stars move away from the cluster center. A similar trend has been noticed by Lee et al. (2013) in their investigation of the clusters NGC 1245 and NGC 2506. A detailed study on the dynamical evolution is presented in Section 5.

### 3.2 Colour-Magnitude Diagram

The identification of the cluster main sequence in the colour-magnitude diagrams (CMDs) allows a model-dependent mass, radius, and distance for each star to be determined. To draw the CMD, we used the area within cluster radius ( $4'.5$ ) as the ‘*cluster region*’ and an equal area outside the cluster radius of  $5'.6$  as the ‘*field region*’. In the left panels of Fig. 5, we constructed calibrated ( $B-V$ ), and ( $V-I$ ) vs  $V$  diagrams of NGC 559 using the stars falling in the cluster region. A similar diagram for the stars in the field region are shown in the middle panels of the same figure.

Since stars in the cluster region are contaminated by the field star population, we adopted a statistical approach to remove the field star contamination. This method is based on a comparison of the cluster and field CMDs. We removed all cluster stars in the ( $V-I$ )/ $V$  CMD which fall within a grid cell of ( $V, V-I$ ) = ( $\pm 0.25, \pm 0.125$ ) of the field stars CMD. A similar removal process was done for the ( $B-V$ )/ $V$  CMD with a grid of ( $V, B-V$ ) = ( $\pm 0.25, \pm 0.10$ ). We iterated the procedure for each star lying on the CMDs of the field region. We were finally left with 462 stars in the

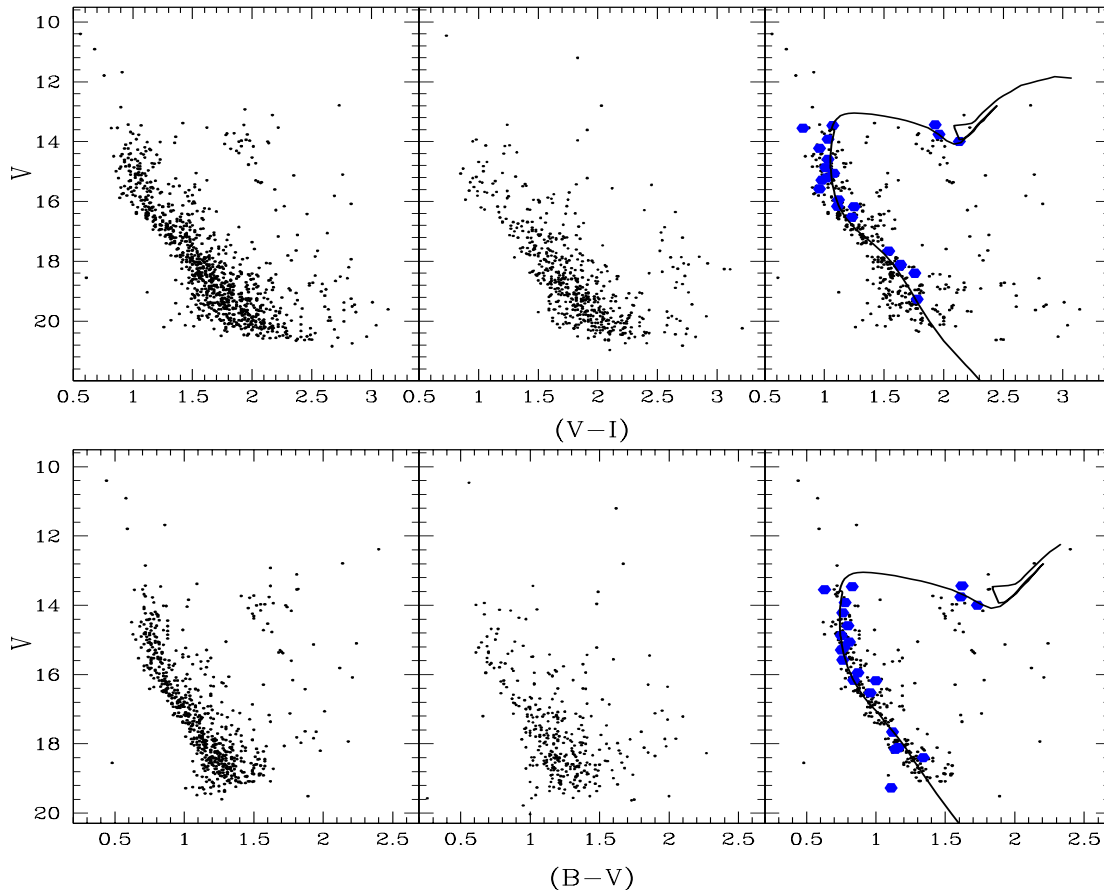


**Figure 5.** The  $(B - V)/V$  and  $(V - I)/V$  CMDs for stars in the cluster region (left panels) and field region (middle panels). The right panels show the same for the stars in the cluster field after statistical subtraction of field stars. The most probable cluster members (see, Table 5) are shown by large filled circles. The solid line represents the best fit isochrone to the cluster MS for  $\log(\text{Age})=8.35$  (see, § 4.3 for detail).

$(V - I)/V$  CMD and 341 stars in the  $(B - V)/V$  CMD. We found more stars in the  $(V - I)/V$  CMD because our photometry goes deeper in the  $V$  and  $I$  bands than in the  $B$  band. The statistically cleaned cluster CMDs are shown in the right hand panels of Fig. 5. The spatial distribution of stars extracted after the statistical subtraction shows that the inner region is dominated by giant and upper-MS stars, whereas the outer region is dominated by low-mass stars. The lack of stars in some pockets is quite evident in the cleaned CMDs. These kind of gaps in MS are not unusual and have been found in many clusters (see detail in Rachford & Canterna 2000). AL02 also noticed a gap at  $M_V \sim 3.5$  mag ( $m_v \sim 18.1$ ) in the cluster NGC 559 similar to the one seen in the present study. This suggests that these gaps could be due to a real lack of cluster members in some magnitude bins.

### 3.3 Mean proper motion

Recently, Roeser et al. (2010) provided a catalogue which lists stellar coordinates with an accuracy of 80–300 mas and absolute proper motion with an accuracy of 4–10 mas yr<sup>-1</sup> for about 900 million stars. A cross-match of these stars with our catalogue using a matching criterion of 1'' resulted

in 1824 stars in common. In Table 4, we provide proper motions of these stars along the RA and DEC directions and their respective errors. Fig. 6 shows the proper motion distribution in the RA-DEC plane.

To determine the mean proper motion of the cluster, we considered those 341 stars which fall in both the cleaned  $(V - I)/V$  and  $(B - V)/V$  CMDs. Among them, 307 stars were found within 1'' of the Roeser et al. (2010) catalogue positions. We determined the mean and  $\sigma$  values of the proper motion in both RA and DEC directions and rejected those stars which fall outside  $3\sigma$  in both the directions. We iterated this procedure until all values fall within  $3\sigma$  of the mean. We were finally left with 229 stars which were used to determine the mean proper motion of the cluster NGC 559. These stars are shown by filled circles in Fig. 6. The mean proper motion of the cluster determined in this way is

$$\bar{\mu}_x = -3.29 \pm 0.35 \text{ mas yr}^{-1}; \quad \bar{\mu}_y = -1.24 \pm 0.28 \text{ mas yr}^{-1}$$

where the uncertainties are standard deviations. A similar matching criteria using UCAC4 catalogue (Zacharias et al. 2013) has given only 167 stars though UCAC4 catalogue provides proper motion with higher accuracy. A  $3\sigma$  clipping



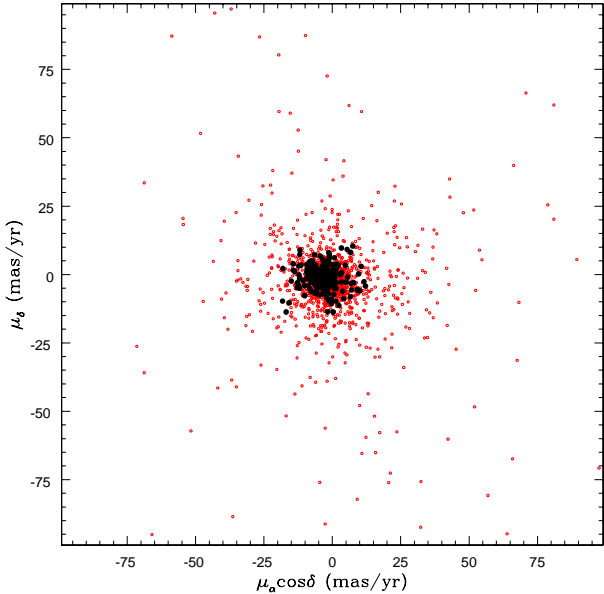


**Figure 6.** The distribution of stars in the  $\mu_x - \mu_y$  plane for which proper motion values are determined in our catalogue and given in Table 4. The 229 stars used to estimate the mean proper motion are shown by filled circles.

analysis done on the proper motions left 145 stars which resulted a mean proper motion of  $\bar{\mu}_x = -4.45 \pm 0.49$  and  $\bar{\mu}_y = 1.65 \pm 0.37 \text{ mas yr}^{-1}$  in RA and DEC directions, respectively. The proper motion for the cluster NGC 559 estimated using two different catalogues are therefore in close agreement within their given uncertainties. From the radial-velocity measurements of 24 stars computed from the data of the Tycho-2 catalog, Loktin & Beshenov (2003) estimated a proper motion of  $\bar{\mu}_x = -1.59 \pm 0.41$  and  $\bar{\mu}_y = -0.52 \pm 0.46 \text{ mas yr}^{-1}$  for the cluster NGC 559, which is lower than the present estimates.

### 3.4 Probable cluster members

Open clusters are mostly located within the densely populated Galactic plane and often contaminated with large numbers of field stars belonging to the disc population. It is therefore essential to discriminate between members and non-members in order to obtain correct cluster parameters. To identify the most-likely cluster members in NGC 559, we first derive different membership probabilities for each star in the cluster field based on their spatial distribution, position in the colour-magnitude diagram and proper motions.

#### 3.4.1 Spatial probability

The spatial probability,  $P_{\text{sp}}$ , is a function of the angular distance of the star from the cluster centre,  $r$ , and is given by

$$P_{\text{sp}} = 1 - \frac{r}{r_c}$$

where  $r_c$  is the angular radius of the cluster. Using  $r_c = 4'.5$  derived in §3.1, we determined  $P_{\text{sp}}$  for all the 960 stars falling within the cluster radius. For  $r \geq r_c$  we assign  $P_{\text{sp}} =$

**Table 5.** The list of 22 most-likely members identified in the cluster NGC 559. These stars were identified using various probability criteria (see, §3.4.3 for detail.)

RA (J2000)	DEC (J2000)	V (mag)	(B-V) (mag)	(V-I) (mag)
01:29:31.07	+63:18:12.5	13.44	1.62	1.93
01:29:32.99	+63:19:35.4	13.46	0.83	1.07
01:29:44.60	+63:18:22.2	13.55	0.63	0.82
01:29:20.89	+63:17:36.4	13.76	1.61	1.96
01:29:22.77	+63:18:20.2	13.92	0.78	1.03
01:29:34.17	+63:19:19.6	14.00	1.73	2.13
01:29:28.30	+63:18:19.0	14.22	0.76	0.96
01:29:36.93	+63:18:30.6	14.59	0.80	1.03
01:29:29.19	+63:19:37.8	14.87	0.75	1.01
01:29:32.73	+63:18:02.3	15.06	0.81	1.08
01:29:25.03	+63:18:41.6	15.21	0.77	1.02
01:29:29.05	+63:18:37.6	15.29	0.75	0.98
01:29:21.37	+63:18:03.1	15.58	0.76	0.96
01:29:38.52	+63:18:02.2	15.95	0.87	1.12
01:29:33.45	+63:16:56.4	16.16	0.84	1.11
01:29:27.26	+63:18:47.5	16.18	1.00	1.25
01:29:39.44	+63:17:15.2	16.53	0.96	1.23
01:29:40.51	+63:18:54.0	17.66	1.12	1.54
01:29:34.39	+63:17:18.7	18.11	1.16	1.64
01:29:32.42	+63:16:53.7	18.16	1.14	1.63
01:29:37.57	+63:18:44.9	18.40	1.34	1.76
01:29:29.26	+63:19:01.4	19.27	1.11	1.78

0. We found 176 stars within the core region of the cluster for which  $P_{\text{sp}} \geq 0.67$ .

#### 3.4.2 Statistical probability

We determine statistical probability which is based on a comparison of the cluster CMD with that of the field CMD, as discussed in §4.3. In this method we removed all the stars in the  $(B-V)/V$  CMD of the cluster field which fall within a grid cell of  $(V, B-V) = (\pm 0.25, \pm 0.10)$ , in the field CMD. After iterating the procedure for each star lying on the CMD of the field region, we found 341 stars for which we assigned statistical probabilities  $P_{\text{st}} = 1$ . For the remaining stars, we assigned  $P_{\text{st}} = 0$ .

#### 3.4.3 Kinematic probability

The kinematic probability,  $P_k$ , is defined as the deviation in the proper motion of stars in both RA and DEC directions with respect to the mean proper motion of the cluster.

Using the method given by Kharchenko et al. (2004), we determined  $P_k$  for each star using

$$P_k = \exp \left\{ -0.25 \left[ \frac{(\mu_x - \bar{\mu}_x)^2}{\sigma_x^2} + \frac{(\mu_y - \bar{\mu}_y)^2}{\sigma_y^2} \right] \right\}$$

where  $\sigma_x^2 = \sigma_{\mu_x}^2 + \sigma_{\bar{\mu}_x}^2$  and  $\sigma_y^2 = \sigma_{\mu_y}^2 + \sigma_{\bar{\mu}_y}^2$ . The mean proper motion of the cluster NGC 559 is taken from our analysis carried out in §3.3. We found 1824 stars for which  $P_k$  could be estimated using the Roeser et al. (2010) catalogue.

To identify the most-likely members in the cluster NGC 559, we considered stars those lie in the core region of the cluster ( $P_{\text{sp}} \geq 0.67$ ), fall within the cleaned CMD ( $P_{\text{st}}=1.0$ ), and proper motion within  $1\sigma$  of the mean proper

**Table 6.** The slopes of the  $(\lambda - V)/(B - V)$  diagrams in the direction of the cluster NGC 559. Normal value in the same colour is given in the bracket.

$\frac{(R-V)}{(B-V)}$	$\frac{(I-V)}{(B-V)}$	$\frac{(J-V)}{(B-V)}$	$\frac{(H-V)}{(B-V)}$	$\frac{(K-V)}{(B-V)}$
$0.62 \pm 0.01$	$1.21 \pm 0.01$	$1.95 \pm 0.02$	$2.50 \pm 0.02$	$2.63 \pm 0.02$
(0.55)	(1.10)	(1.96)	(2.42)	(2.60)

motion ( $P_k \geq 0.60$ ). We identified 22 such stars in our catalogue which fulfill above criteria. These criteria are conservative in the sense that they confer membership status to the selected stars, but it does not mean that other stars are non-members. The positions of these stars along with their magnitude, and colours are given in Table 5. To determine robust cluster parameters for NGC 559, these stars were preferentially used in our analysis as explained in the following section.

## 4 CLUSTER PARAMETERS

### 4.1 Reddening law and two-colour-diagrams

Though the normal reddening law,  $R_V = \frac{A_V}{E(B-V)} = 3.1$ , is valid for lines of sight that do not pass through dense clouds (Snedden et al. 1978), clusters associated with gas and dust or behind the dusty Galactic spiral arms may give a different value of  $R_V$ . To investigate the nature of the reddening law, Chini & Wargau (1990) showed that the TCDs of the form  $(\lambda - V)/(B - V)$  can be used, where  $\lambda$  is any broad-band filter. The slope of the TCD distinguishes normal extinction produced by grains in the diffuse interstellar medium from that caused by abnormal dust grains (Pandey et al. 2000). We studied the reddening law in the cluster NGC 559 by drawing  $(\lambda - V)/(B - V)$  diagrams for the  $\lambda = R, I, J, H$  and  $K$  bands as shown in Fig. 7. The slope,  $m_{\text{cluster}}$ , was determined by fitting a linear relation in the TCD for the stars in the cluster region and a best fit determined after a  $3\sigma$ -clipping iteration. The estimated values of  $m_{\text{cluster}}$  for all five colours are given in Table 6 along with their normal values. To derive the value of total-to-selective extinction  $R_{\text{cluster}}$  in the direction of NGC 559, we used the approximate relation (cf. Neckel & Chini 1981)

$$R_{\text{cluster}} = \frac{m_{\text{cluster}}}{m_{\text{normal}}} \times R_{\text{normal}}$$

Using  $R_{\text{normal}} = 3.1$ , we estimated  $R_{\text{cluster}}$  in different passbands to be  $3.1 < R_{\text{cluster}} < 3.5$  which is marginally higher than the normal value. The reddening law in the direction of the cluster is found to be normal at longer wavelengths but anomalous at shorter wavelengths.

### 4.2 Reddening determination: $(U - B)$ vs $(B - V)$ TCD

The reddening,  $E(B - V)$ , in the cluster region is normally determined using the  $(U - B)/(B - V)$  two-colour diagram (TCD). Out of 2393 stars in our catalogue, we found only 501 stars for which all the  $U, B$  and  $V$  magnitudes are available. Among them, we considered only 275 stars within the cluster which have a  $U$  band photometric error less than

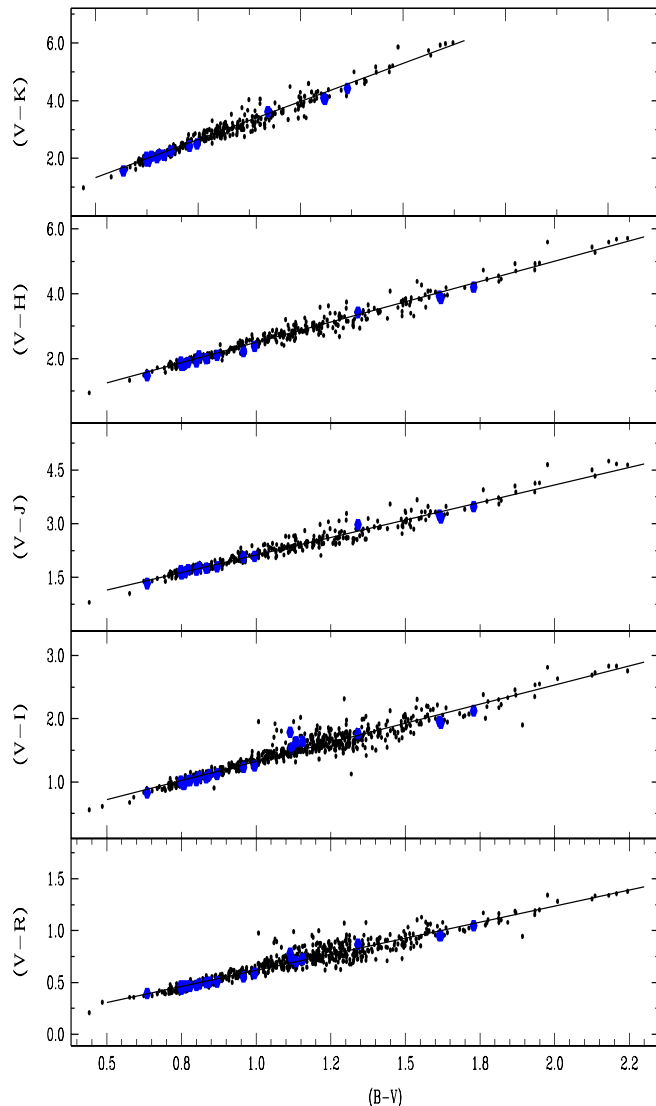


**Figure 7.** The  $(\lambda - V)/(B - V)$  two-colour diagram for the stars within cluster region. The most probable cluster members are shown by large filled circles. The continuous lines represent the slope determined through least square linear fit.

0.05. The resulting TCD is shown in Fig. 8. As mentioned in the previous section, the normal reddening law is not applicable at shorter wavelengths. Therefore, we have fitted intrinsic zero-age main sequence (ZAMS) isochrones of solar metallicity (Marigo et al. 2008) to the observed MS stars by shifting  $E(B - V)$  and  $E(U - B)$  along different values of the reddening vector  $\frac{E(U-B)}{E(B-V)}$ . A visual inspection shows that the best fit is achieved for  $\frac{E(U-B)}{E(B-V)} = 0.84 \pm 0.01$ . This gives a mean reddening of  $E(B - V) = 0.82 \pm 0.02$  in the direction of NGC 559 as shown by a solid line in Fig. 8. In determining the reddening, we used only stars having colours corresponding to spectral classes earlier than A0 because stars having later spectral types are more affected by metallicity and background contamination (Hoyle et al. 2003). The colour excess obtained in the present study is in good agreement with the value  $E(B - V) = 0.81 \pm 0.05$  given by



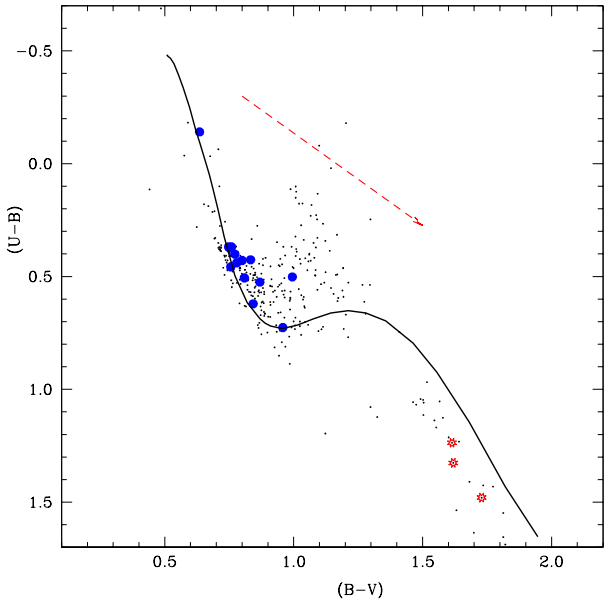


**Figure 8.** The  $(U - B)$  versus  $(B - V)$  diagram for the stars in NGC 559. The small dots represent the stars which lie within the cluster boundary and have a  $U$ -band photometric error less than 0.05. Filled circles are the most probable cluster members. The 3 stars shown in red colour represent red giants belonging to the cluster but not considered in the reddening estimation. The thick dashed arrow represents the slope (0.84) and direction of the reddening vector. The solid line represents the ZAMS with solar metallicity taken from the Marigo et al. (2008) shifted for  $E(B - V) = 0.82$ .

AL02, but higher than  $0.68_{-0.12}^{+0.11}$  obtained by MN07. Using the Johnson & Morgan (1953)  $Q$ -method for stars earlier than A0 ( $(B - V) < 0.84$ ), we determined the reddening of each star. The reddening distributions of these stars show that reddening is uniform over the whole cluster.

Considering  $R_{\text{normal}} = 3.1$ , we estimated a higher value of  $R_{\text{cluster}} = 3.6$  for ultraviolet wavelengths. This further suggests an anomalous reddening law at shorter wavelengths in the direction of NGC 559. Chini & Wargau (1990) pointed out that both larger and smaller size grains may increase  $R_{\text{cluster}}$ . However, some of the recent studies (e.g., Whittet et al. 2001, Pandey et al. 2008 and references therein) suggest that a value of  $R_{\text{cluster}}$  higher than the normal is indicative of the presence of larger dust grains. As NGC 559 is situated behind the Perseus arm, a high reddening and anomalous reddening law is not surprising.

### 4.3 Distance and Age determination

The distance and age of NGC 559 can be estimated by visual fitting of theoretical isochrones to the MS. For this purpose we used  $(B - V)/V$  and  $(V - I)/V$  CMDs shown in the right panels of Fig. 5. The stars show a broad but clearly distinct MS in the CMD. The width is mainly caused by cluster binaries and field stars. There are a few stars scattered towards the red side of the CMDs. We suspect these may be foreground field stars which have remained due to incomplete subtraction of the field star contamination. We presume most of them belong to the Perseus spiral arm. In order

to obtain the most reliable estimates of the cluster parameters, we identified those stars in the cleaned CMDs which lie inside the core region and have proper motions within  $1\sigma$  of the mean proper motion of the cluster. These stars are shown by the blue filled circles in Fig. 5. We used stellar evolutionary isochrones published by the Padova group<sup>3</sup> (Marigo et al. 2008) to estimate the cluster age and distance. We fixed the reddening to the value estimated in § 4.2. A simultaneous best fit was made of the isochrones in the bluest envelope of the  $(B - V)/V$  and  $(V - I)/V$  CMDs, corrected for a mean reddening of  $E(B - V) = 0.82$  and  $E(V - I) = 1.12$  assuming  $\frac{E(V - I)}{E(B - V)} = 1.37$  (Schlegel et al. 1998). This gives an age of  $\log(\text{Age}) = 8.35 \pm 0.05$  and an apparent distance modulus of  $(m - M) = 14.80 \pm 0.05$  for NGC 559. The errors in age and distance are strongly influenced by a few blue and red supergiants in the CMDs.

As we have seen in § 4.1 and § 4.2, that the total-to-selective extinction in optical region varies from 3.4 to 3.6. We adopted a mean value of  $R_V = 3.5 \pm 0.1$  as the total-to-selective extinction in the direction of NGC 559. Assuming a total extinction of  $A_V = R_V \times E(B - V)$ , the reddening-free distance modulus is estimated as  $(V_0 - M_V) = 11.93 \pm 0.20$ , which corresponds to a distance of  $2.43 \pm 0.23$  kpc for NGC 559. The linear diameter of the cluster is estimated to be  $6.4 \pm 0.4$  pc. Since the cluster lies very close to the Galactic plane, a large foreground extinction of about  $E(B - V) = 0.56$  is expected in that direction (Schlegel et al. 1998, Joshi 2005).

The position of NGC 559 in Galactic coordinates is  $l = 127^\circ.2, b = +0^\circ.75$ . Assuming that the Sun is at a distance of 8.5 kpc from the Galactic center, the Galactocentric rectangular coordinates of NGC 559 are  $X \sim 1.88$  kpc,  $Y \sim 1.44$  kpc,  $Z \sim +30.9$  pc and a Galactocentric distance of  $\sim 10.1$  kpc for the cluster. This places NGC 559 just outside the Perseus spiral arm. The distance of the cluster from the Galactic plane is smaller than the typical scale height of the thin disk ( $\approx 75$  pc). This is in agreement with Joshi (2007) which found that most of the OCs younger than about 300 Myr lie somewhere within  $\pm 100$  pc of the Galactic Plane.

### 4.4 Interstellar extinction in the near-infrared

To determine interstellar extinction in the near-IR, we used 370 stars for which  $VJK$  magnitudes were available in our catalogue. The  $(V - K)/(J - K)$  diagram is shown in Fig. 9. We used the normal reddening law for the infra-red colours, as given in Table 6, and shifted the stars along the reddening vector  $\frac{E(J - K)}{E(V - K)} = 0.173$  using solar metallicity isochrones given by the Marigo et al. (2008). The best fit to points in the  $(V - K)/(J - K)$  diagram gives a colour excess of  $E(V - K) = 2.14 \pm 0.02$  and  $E(J - K) = 0.37 \pm 0.01$  by minimizing  $\chi^2$ . The theoretical isochrone shifted by the above values is shown by the solid line in Fig. 9. Using the Whittet & van Breda (1980) relation for  $R_K = 1.1E(V - K)/E(B - V)$ , which is insensitive to the reddening law, we obtained  $E(B - V) = 0.76 \pm 0.04$  for the reddening in NGC 559. This is close to  $E(B - V) = 0.82 \pm 0.02$  determined using the  $(U - B)/(B - V)$

<sup>3</sup> <http://pleiadi.pd.astro.it/>

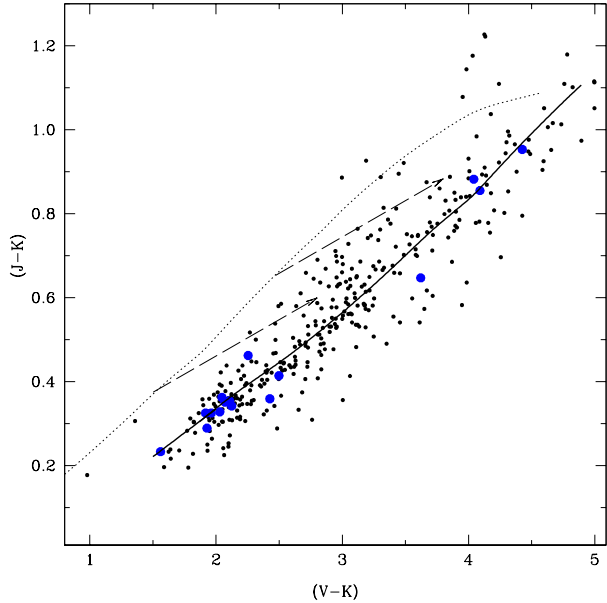


**Figure 9.** The  $(V - K)/(J - K)$  colour-colour diagram for stars within the cluster boundary. Filled circles are the most probable cluster members. The dotted line is the solar metallicity isochrone for  $\log(\text{Age})=8.35$ , while the two dashed lines indicate the direction of the normal reddening vector. The solid line is obtained by using reddenings of  $E(V - K) = 2.14$  and  $E(J - K) = 0.37$ .

**Table 7.** Fundamental parameters of the cluster NGC 559 as determined in the present study.

Cluster parameters	
RA(2000)	01:29:32.33
DEC(2000)	+63:18:14.5
$R_{\text{core}}$	$1.3 \pm 0.3$ arcmin
$R_{\text{cluster}}$	$4.54 \pm 0.20$ arcmin
Mean $E(B - V)$	$0.82 \pm 0.02$ mag
$(m - M)_v$	$14.8 \pm 0.05$ mag
$\bar{\mu}_\alpha$	$-3.29 \pm 0.35$ mas/yr
$\bar{\mu}_\delta$	$-1.24 \pm 0.28$ mas/yr
$\log(\text{Age}/\text{yr})$	$8.35 \pm 0.05$
Total-to-selective extinction $R_V$	$3.5 \pm 0.1$
Distance	$2.43 \pm 0.23$ kpc
Diameter	$6.4 \pm 0.4$ pc

TCD. The agreement between two complementary methods suggests that our values are robust.

The fundamental parameters derived for NGC 559 in this study are summarized in Table 7.

#### 4.5 Comparison to previous results

NGC 559 has been studied in the past by various authors. Lindoff (1969) found it to be a very old cluster with an age of about 1000 Myr, while Jennens & Helfer (1975) estimate the age at only 100 Myr. Both studies used photoelectric photometry. Grubissich (1975), Lynga (1987), AL02 and MN07, all estimated the cluster age at  $\log(\text{Age}) = 8.7 \pm 0.1$ . In this paper we used only the most probable cluster members to estimate  $\log(\text{Age}) = 8.35 \pm 0.05$ .

The distance of the cluster is estimated to be about 1.3 kpc (Lindoff 1969), 6.3 kpc (Jennens & Helfer 1975), and 1.15 kpc (Lynga 1987). The recent CCD study by AL02 and MN07 determined a distance of  $2.3 \pm 0.3$  and  $2.17^{+0.56}_{-0.82}$  kpc respectively. The latter value is close to the distance of  $2.43 \pm 0.22$  kpc determined in the present study. Previous estimates of reddening,  $E(B - V)$ , are about 0.45 (Lindoff 1969),  $0.62 \pm 0.17$  (Jennens & Helfer 1975), 0.54 (Lynga 1987), and  $0.68^{+0.11}_{-0.12}$  (MN07). However, AL02 obtained a higher value of  $E(B - V) = 0.81 \pm 0.05$ , which is in good agreement with our value of  $0.82 \pm 0.02$ .

## 5 DYNAMICAL STUDY OF THE CLUSTER

The dynamical properties of the cluster can be studied by determining the luminosity and mass functions of the cluster members.

### 5.1 Luminosity function

The luminosity function (LF) is the total number of cluster members in different magnitude bins. After correcting for the data completeness to both cluster and field regions, the number of probable cluster members was obtained by subtracting the contribution of field stars from stars in the cluster region. The estimated number of stars in each magnitude bin for both the cluster ( $N_C$ ) and field regions ( $N_F$ ) are given in Table 8. To determine the photometric LFs in  $(V - I)/V$  and  $(B - V)/V$  CMDs, we subtracted  $N_F$  from  $N_C$  and resultant probable members ( $N_P$ ) are given in the 4th and 7th columns of Table 8, respectively.

### 5.2 Mass function

The initial mass function (IMF) is defined as the distribution of stellar masses per unit volume in a star formation event. Along with the star formation rate, the IMF determines the subsequent evolution of clusters (Kroupa 2002). Since the direct determination of the IMF is not possible due to the dynamical evolution of stellar systems, we derive the mass function (MF), which is the relative number of stars per unit mass and can be expressed by a power law  $N(\log M) \propto M^\Gamma$ . The slope,  $\Gamma$ , of the MF can be determined from

$$\Gamma = \frac{d \log N(\log m)}{d \log m}$$

where  $N \log(m)$  is the number of stars per unit logarithmic mass. The masses of probable cluster members can be determined by comparing observed magnitudes with those predicted by a stellar evolutionary model if the age, reddening, distance and metallicity are known.

As seen in Fig. 5, the  $(V - I)/V$  CMD goes deeper than the  $(B - V)/V$  CMD, so we used the former to determine the MF of the cluster. The main factors that limit the accuracy of the MF are incompleteness and field star contamination. While the central region of the cluster may be affected by data incompleteness, the outer region is more likely to be affected by field star contamination. After statistically correcting for the field star contamination, we determined the MF in three regions i.e., the core region ( $r \leq 1'.3$ ), the corona

**Table 8.** Luminosity Functions of the stars in the  $(V - I)/V$  and  $(B - V)/V$  CMDs of the cluster and field regions.  $N_C$  and  $N_F$  denote the number of stars in a magnitude bin in the cluster and field regions.  $N_P$  ( $N_C - N_F$ ) gives the difference between MS stars between the cluster and field regions.

V range (mag)	(V-I)/V CMD			(B-V)/V CMD		
	$N_C$	$N_F$	$N_P$	$N_C$	$N_F$	$N_P$
12-13	0	0	0	3	0	3
13-14	8	2	6	5	0	5
14-15	8	0	8	12	2	10
15-16	24	6	18	36	5	31
16-17	68	14	54	66	11	55
17-18	73	33	40	48	33	15
18-19	91	41	50	65	30	35
19-20	80	38	42	9	4	5
20-21	46	38	8	-	-	-

**Table 9.** The mass function of the cluster NGC 559 derived from  $(V - I)/V$  CMD.

V Range (mag)	Mass Range ( $M_\odot$ )	$\bar{m}$ ( $M_\odot$ )	$N$	$\log(m)$	$\log(\phi)$
13-14	3.67-3.44	3.61	2	0.557	1.854
14-15	3.44-2.86	3.21	7	0.506	1.939
15-16	2.86-2.20	2.61	18	0.417	2.200
16-17	2.20-1.73	2.00	53	0.301	2.710
17-18	1.73-1.40	1.63	43	0.213	2.665
18-19	1.40-1.10	1.30	49	0.114	2.670
19-20	1.10-1.00	1.10	42	0.041	3.006
20-21	1.00-0.80	0.95	32	-0.022	2.519

**Table 10.** MF slope ( $\Gamma$ ) for the stars in the mass range of about 1.0 to 3.7  $M_\odot$

Region (Radial distance)	$\Gamma$
core ( $r \leq 1'.3$ )	-1.64 $\pm$ 0.62
corona ( $1'.3 < r \leq 4'.5$ )	-2.14 $\pm$ 0.30
cluster ( $r \leq 4'.5$ )	-2.12 $\pm$ 0.31

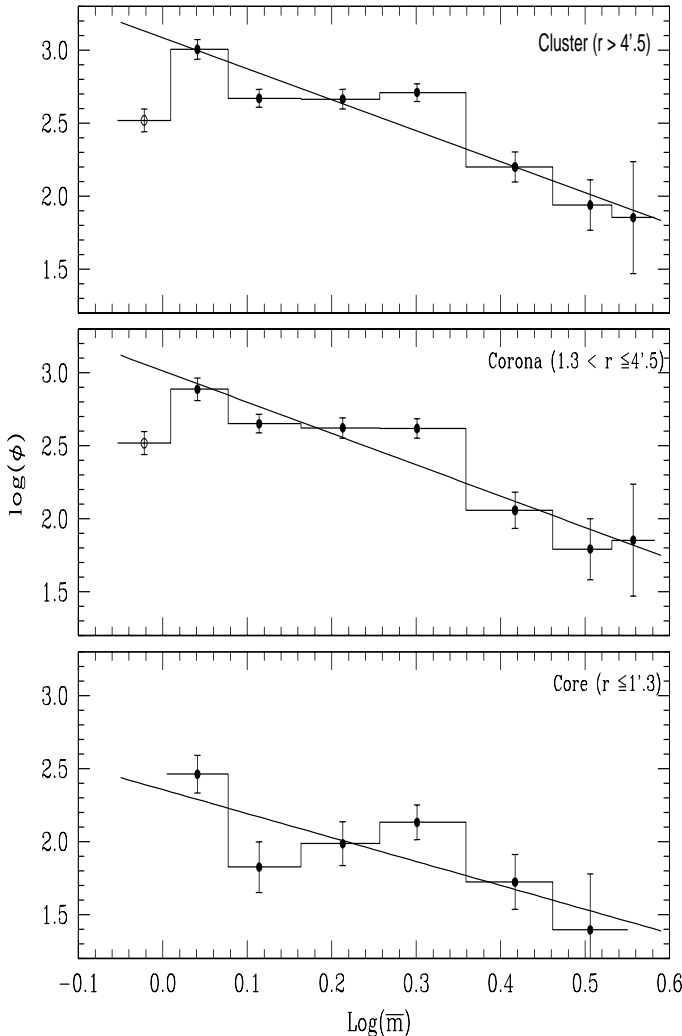


**Figure 10.** MF derived for the core region (lower panel), corona (middle panel), and whole cluster region (upper panel). The error bars represent  $1/\sqrt{N}$  errors. The continuous line is the fit to the data excluding the points shown by open circles.

( $1'.3 < r \leq 4'.5$ ), and the whole cluster region ( $r \leq 4'.5$ ). The MF determined for the cluster region is given in Table 9. Fig. 10 shows the MF in the cluster fitted for the MS stars with masses  $0.8 \leq M/M_\odot < 3.7$ . The error bars were calculated assuming Poisson statistics. In determining the slope, we have considered only those data points which are shown by filled circles in Fig. 10. The slope of the MF ( $\Gamma$ ) in the mass range  $1.0 \leq M/M_\odot < 3.7$  in each region is calculated using a least square method and shown by the solid line in the figure. Table 10 summarizes the MF slopes in the cluster for all three regions. For the mass range  $0.4 < M/M_\odot < 10$ , the classical value derived by Salpeter (1955) for the MF slope is -1.35. The MF slope in the core region is in agreement with the Salpeter MF slope within the given uncertainty, but it is steeper for the corona and cluster regions. This suggests a preferential distribution of relatively massive stars towards the central region of the cluster. When we determined the MF slopes for two extreme age limits of the cluster considering the uncertainty in our age determinations, we found that the MF slope is slightly dependent on the age of the cluster, and varies by a maximum of  $\sim 20\%$ .

It is worth pointing out that the mass range for probable MS stars in this cluster is quite small. It is possible that some of the low mass stars may have escaped from the cluster as a result of stellar encounters between stars of different masses. On the other hand, the initially massive stellar members of the cluster have now evolved and may possibly be white dwarfs or have undergone supernova explosions. Very deep photometry will be required to detect white dwarfs or supernova remnants, if present.

### 5.3 Mass Segregation

There is ample proof of mass segregation in star clusters, i.e. a tendency of higher-mass stars to approach towards inner region and lower-mass stars towards outer region of

**Table 11.** Parameters used to estimate  $T_E$  for the cluster NGC 559.

Probable members ( $N$ )	202
Total cluster mass	344 $M_\odot$
Cluster half radius ( $R_h$ )	2.3 pc
Mean stellar mass ( $\bar{m}$ )	1.7 $M_\odot$
Dynamical relaxation time ( $T_E$ )	19.2 Myrs
Age of the cluster	224 Myrs

the cluster. This appears to be a result of equipartition of energy through stellar encounters (e.g., Mathieu & Latha, 1986, Sagar et al. 1988, Pandey et al. 2001). To understand if mass segregation is an imprint of the star formation process in the cluster and/or a result of dynamical evolution, we determined the dynamical relaxation time,  $T_E$ . This is the time in which individual stars in the cluster exchange energies and their velocity distribution approaches the Maxwellian equilibrium. It can be expressed as

$$T_E = \frac{8.9 \times 10^5 (NR_h^3 / \bar{m})^{1/2}}{\log(0.4N)}$$

where  $T_E$  is in Myr,  $N$  is the total number of cluster members,  $R_h$  is the radius (in parsecs) containing half of the cluster mass and  $\bar{m}$  is mean mass of the cluster members in solar units (cf. Spitzer & Hart, 1971). We estimated a total of 202 MS stars in the mass range  $0.8 \leq M/M_\odot < 3.7$ . The total mass of the cluster is obtained by subtracting the total stellar mass in the field region from the cluster region. This results in a total mass of  $\sim 344 M_\odot$  for NGC 559, which gives an average mass of  $\sim 1.7 M_\odot$  per star. The contribution of the low-mass stellar population is critical for constraining the total cluster mass, which is crucial in understanding the dynamical evolution and the long-term survival of a cluster (e.g., de Grijs & Parmentier 2007, and references therein). We can not rule out the possibility of poor subtraction of field stars from the cluster or an observing bias against detecting low-mass stars which might result in underestimating the total mass of the cluster. Therefore the present value may be taken as a lower limit for the cluster mass, while the estimated mean stellar mass can be taken as an upper limit.

It can be seen that the half-radius of the cluster,  $R_h$ , plays an important role in the determination of the dynamical relaxation time,  $T_E$ . Unfortunately, this quantity is unknown for most clusters and is generally taken as half of the total cluster radius. Nevertheless, we can estimate  $R_h$  by taking advantage of the statistical removal of field stars from the field region and knowledge of the approximate stellar masses using stellar isochrones. The value of  $R_h$  determined in this way is  $\sim 2.3$  pc, which is  $\sim 70\%$  of the cluster radius. A  $R_h$  value larger than half of the cluster radius suggests that inner region has a deficiency of massive stars which have now evolved. We estimated the dynamical relaxation time  $T_E = 19.2$  Myr for NGC 559. However, cluster members fainter than the limiting  $V$  magnitude of our observations results in a decrease of  $N$  and an increase of  $\bar{m}$ , leading to an underestimation of  $T_E$ . Therefore,  $T_E$  obtained in this way should be regarded as a lower limit. The values used in the estimation of  $T_E$  are summarized in Table 11.  $T_E$  determined in the present study is much smaller than the present age of about 224 Myr. We conclude, therefore, that NGC 559 is a dynamically relaxed cluster.

## 6 CONCLUSION AND SUMMARY

We present results of an ongoing photometric survey in order to determine the structure, and astrophysical and dynamic evolution parameters of the intermediate age galactic cluster NGC 559. We present a comprehensive *UBVR1JHK*-proper motion catalogue for 2393 stars down to about  $V = 21.4$  mag observed in a  $\sim 13' \times 13'$  field centered on the cluster. Fundamental parameters, such as core and cluster radius, reddening  $E(B - V)$ , age, distance modulus and mean proper motion were obtained using optical and near-IR photometry and proper motions. We analysed the cluster membership using criteria based on distance from the cluster center, position in the CMD, and proper motions. The membership probabilities of all stars in the field of the cluster are presented. We found 22 stars which are the most probable cluster members. Our study indicates a distance of  $2.43 \pm 0.23$  kpc, a diameter of  $6.4 \pm 0.4$  pc and an age of  $224 \pm 25$  Myr. The cluster is found to be heavily reddened with  $E(B - V) = 0.82 \pm 0.02$ . The mean proper motion was estimated to be  $\mu_x = -3.29 \pm 0.35$  mas yr $^{-1}$ ,  $\mu_y = -1.24 \pm 0.28$  mas yr $^{-1}$ . Our analysis suggests that the cluster is slightly younger and more reddened than previously thought. It is important to note that because we limit determinations to the most probable cluster members, the errors in the estimates of various cluster parameters has been considerably reduced.

The reddening law in the direction of the cluster was found to be normal at longer wavelength but anomalous at shorter wavelengths. In general, we found a slightly higher total-to-selective extinction  $R_V = 3.3$  towards NGC 559. The larger value of  $R_V$  could be caused by a bigger than average grain size. Polarimetric data would be useful to ascertain the size and behaviour of the dust grains. From the combined optical and near-infrared data, we obtained a colour excesses of  $E(V - K) = 2.14 \pm 0.02$ ,  $E(J - K) = 0.37 \pm 0.01$ , and  $E(B - V) = 0.76 \pm 0.04$ , in the direction of NGC 559.

The MF for MS stars in the cluster is not uniform over the entire region and found in the range  $-1.64 \geq \Gamma \geq -2.14$  for the mass range  $1.0 \leq M/M_\odot < 3.7$ . The MF slope of the core region is in agreement with the Salpeter value, but it is found steeper in the corona and in the cluster as a whole. This suggests mass segregation in MS stars due to the dynamical evolution of the cluster. A deficiency of low-mass stars as well as very massive stars was found in the core region of the cluster. The age of the cluster was found to be much higher than the relaxation time of 19.2 Myr, which implies that the cluster is dynamically relaxed. An improvement in the cluster parameters and knowledge of dynamical evolution should allow a better understanding of star formation in NGC 559.

In a forthcoming paper, we will report on stellar variability in NGC 559 from 35 nights taken over 3 years during 2010 to 2012.

## ACKNOWLEDGMENTS

The authors thank the anonymous referee for useful comments that improved the scientific content of the paper. We acknowledge the suggestions given by Dr. Ramakant Singh Yadav. This study has made use of data from the Two Mi-

cron All Sky Survey, which is a joint project of the University of Massachusetts; the Infrared Processing and Analysis Center/California Institute of Technology, funded by the National Aeronautics and Space Administration and the National Science Foundation.

## REFERENCES

- [42] Ann H. B., Lee, S. H., 2002, JKAS, 35, 29 (AL02)
- [2001] Carpenter J. M., 2001, ApJ, 121, 2851
- [42] Carraro G., Villanova S., Demarque P., Moni Bidin C., McSwain M. V., 2008, MNRAS, 386, 1625
- [42] Chini R., Wargau W. F., 1990, A&A, 227, 213
- [42] de Grijs R., Parmentier G., 2007, ChJA&A, 7, 155
- [42] Grubissich C., 1975, A&AS, 21, 99
- [2003] Hoyle F., Shanks T., Tanvir N. R., 2003, MNRAS, 345, 269
- [42] Jennens P. A., Helfer H. L., 1975, MNRAS, 172, 681
- [42] Johnson H. L., Morgan W. W., 1953, ApJ, 117, 313
- [42] Joshi Y. C., 2005, MNRAS, 362, 1259
- [42] Joshi Y. C., 2007, MNRAS, 378, 768
- [42] Joshi Y. C., Joshi S., Kumar B., Mondal S., Balona L. A., 2012, MNRAS, 419, 2379
- [42] Kaluzny J., Udalski A., 1992, Acta Astron., 42, 29
- [42] Kharchenko N. V., Piskunov A. E., Röser S., Schilbach E., Scholz R.-D., 2004, Astron. Nachr., 325, 740
- [42] King I., 1966, AJ, 71, 64
- [42] Kroupa P., 2002, Science, 295, 82
- [42] Lada C. J., Lada E. A., 2003, ARA&A, 41, 57
- [42] Landolt A. U., 1992, AJ, 104, 340
- [42] Lee S. H., Kang Y.-W., Ann H. B., 2013, MNRAS, 432, 1672
- [42] Lindoff U., 1969, Arkiv astron, 5, 221
- [42] Loktin A. V., Beshnov G. V., 2003, ARep, 47, 6
- [42] Lynga G., 1987, Catalogue of Open Cluster Data, Centre des Données Stellaires, Strasbourg
- [42] Maciejewski G., Niedzielski, A., 2007, A&A, 467, 1065 (MN07)
- [42] Marigo P., Girardi L., Bressan, A., et al., 2008 A&A, 482, 883
- [1986] Mathieu R. D., Lathen D. W., 1986, AJ, 92, 1364
- [42] Neckel T., Chini R., 1981, A&A, 45, 451
- [42] Pandey A. K., Ogura K., Sekiguchi K., 2000, PASJ, 52, 847
- [42] Pandey A. K., Nilakshi, Ogura K., Sagar R., Tarusawa K., 2001, A&A, 374, 504
- [42] Pandey A. K., Sharma S., Ogura K., et al., 2008, MNRAS, 383, 1241
- [42] Rachford B. L., Canterna R., 2000, AJ, 199, 1296
- [42] Roeser S., Demleitner M., Schilbach E., 2010, AJ, 139, 2440
- [42] Ruprecht J., 1966, Bull. of the Astron. Inst. of Czechoslovakia, 17, 33
- [42] Russeil D., Adami C., Georgelin Y. M., 2007, A&A, 470, 161
- [42] Sagar R., Miakutin V. I., Piskunov A. E., Dlužnevskaja O. B., 1988, MNRAS, 234, 831
- [42] Salpeter E. E., 1955, ApJ, 121, 161
- [42] Skrutskie M. F., Cutri R. M.; Stiening R., et al., 2006, AJ, 131, 1163
- [42] Schlegel D. J., Finkbeiner D. P., Davis M., 1998, ApJ, 500, 525
- [42] Sneden C., Gehrz R. D., Hackwell J. A., York D. G., Snow T. P., 1978, ApJ, 223, 168
- [42] Spitzer L., Hart M. H., 1971, ApJ, 164, 399
- [42] Stetson P. B., 1987, PASP, 99, 191
- [42] Trumpler R. J., 1930, Lick Obs. Bull, 14, 154
- [42] Whittet D. C. B., van Breda I. G., 1980, MNRAS, 192, 467
- [42] Whittet D. C. B., Gerakines P. A., Hough J. H., Shenoy S. S., 2001, ApJ, 547, 872
- [42] Yadav R. K. S., Bedin L. R., Piotto G., et al., 2008, A&A, 484, 609
- [42] Zacharias N., Finch C.T., Girard T.M., et al., 2013, AJ, 145, 44